A chemiresistive gas sensor for sensitive detection of SO_2 employing Ni-MOF modified –OH-SWNTs and –OH-MWNTs

Published: 02 February 2021

Volume 127, article number 157, (2021) Cite this article

Applied Physics A

Aims and scope

Submit manuscript

Nikesh Ingle, Pasha Sayyad, Megha Deshmukh, Gajanan Bodkhe, Manasi Mahadik, Theeazen Al-Gahouari, Sumedh Shirsat & Mahendra D. Shirsat

Abstract

Sulfur dioxide (SO_2) is prominent as hazardous gas owing to its unpropitious effects on the ecosystem. In this report, a flexible SO_2 gas sensor is reported by solvothermally synthesized crystalline nickel(II)benzenetricarboxylate metal–organic framework (Ni-MOF) modified with hydroxyl group (–OH) activated single wall carbon nanotubes (SWNTs) and multi-

walled carbon nanotubes (MWNTs), respectively. Introduction of −OH-SWNTs and −OH−MWNTs played crucial role in the improvement in electrical and morphological properties of Ni-MOF as well as boosted the sensing ability toward SO_2 gas at room temperature. The structural and spectroscopy properties of pristine Ni-MOF, Ni-MOF/−OH−SWNTs and Ni-MOF/−OH-MWNTs were studied by X-Ray diffraction (XRD) and Fourier-transform infrared spectroscopy (FTIR), respectively. Atomic force microscopy (AFM) and field emission scanning electron microscope (FESEM) were used for the morphological analysis of synthesized material. The selective response of Ni-MOF/−OH-SWNTs and Ni-MOF/−OH-MWNTs toward SO_2, NO_2, NH_3 and CO analytes (0.5−15 ppm) was withal studied by monitoring the changes in electrical resistance of the material at room temperature. The present study reveals that doping of −OH-SWNTs and −OH-MWNTs into the MOF leads to efficient increment in the sensing characteristics. The composite of Ni-MOF/−OH-SWNTs exhibited better sensing response (10 s) with less recovery time (30 s) for 1 ppm concentration along with considerable sensitivity (0.9784) and selectivity toward SO_2 gas.

1 Introduction

In today's era environment protection interest is substantially grown in the human community from numerous air pollutants engendered from combustion exhaust. Sulfur dioxide (SO_2), nitrogen dioxide (NO_2), ammonia (NH_3), carbon monoxide (CO), other volatile organic compounds (VOCs) relinquished from prodigious industrial progress that uses sulfur, carbon and nitrogen holding compounds, such as fossil fuels [1,2,3,4,5] are toxic, irritating besides above permissible exposure limit (PEL) mentioned by occupational safety and health administration (OSHA). These gases play a vital role in chemical industries in oil refining, coal burning and several indoor and outdoor activities [1, 2, 6, 7] and further get greatly exposed in the environment. Every day an ample number of gases become exposed in the ecosystem by one and many reasons. Apart from these gases, SO_2 is one of the major hazardous gases contributes to infrequent environmental degradation activities such as acid precipitation, haze formation and visibility degradation. However, day by day increasing health issues due to the contaminated environment is danger alarm for human being as well as the whole ecosystem to pursuit for significant solutions which can give relief to the society. Most importantly, we cannot stop breathing; moreover, we can rely on the designators which can provide signals of hazard-free places for the safety and protection for human beings. So it is an exigent need for development of room temperature operated gas sensors undergoing idyllic characteristics of sensor response time, recovery time and sensitivity using cost-effective products to reach in economically poor sectors also. In the twenty-first century, the demand for real-time, low cost and small size devices [8,9,10] has been continuously initiating for gas sensing applications and to monitor various parameters in the environment [1, 2, 6, 8, 9, 11, 12].

From last few decades, organic conducting polymers (OCPs), carbon nanomaterials (graphene, carbon nanotubes, nanowires, etc.), metalloporphyrins, metal oxides, etc., [1, 2, 4, 13,14,15,16,17,18] are most explored materials for research and industrial communities due to their ideal electrical, chemical, mechanical and morphological properties. These materials secured their place in sensor technology owing to their above-mentioned properties; however, despite all favorable properties still these materials have some unresolved limitations like huge response and recovery time, sensing at high temperature, instability at the normal environment, etc. [19,20,21].

However, to overcome all these above-mentioned issues researchers are optimistic toward the utilization of favorable properties of these individual materials by adopting the composition of these materials and overcoming their limitations. On that line, carbon nanotubes (CNTs) are widely accepted material among the research community as an excellent platform for sensing applications. Interaction between CNTs and gas molecules is responsible for tempting the electronic and mechanical properties as well as the thermal stability of CNTs. The CNTs are chemically inert having architecture of large surface-to-volume ratio provided by the hollow cores and outside walls of nanotubes, offering them enormous gas absorptive possessions. CNTs are possible to make highly interactive through an activation with acidic groups, for the achievement of desirable sensitivity toward gas analytes. Moreover, CNTs have undergone properties like less power consumption, cost-effectiveness, high compatibility with microelectronic processing, etc. All these desirables offer CNTs as the ultimate scope for the enrichment of their sensing characteristics [22,23,24,25,26].

On the other hand, MOFs have secured their place in the group of advanced materials owing to their tunable properties, highly porous structure along with large specific surface area and thermal stability as well [27,28,29,30]. MOFs are known as porous coordination polymers built a network from central metal coordinated with organic ligands. Such networking copolymers are highly demanding for catalysis, gas storage, sensing, drug delivery, adsorption and separation, etc. [31,32,33,34,35]. The MOFs possess ultrahigh surface area (~7000 m^2/g) [36] with a microporous structure [37], highly desirable for sensitive gas adsorption phenomena. In spite of all these desirable properties, MOFs are insulators in nature [38, 39]. More recently, pG-Cu BTC, pG-UiO 66 and pG-ZIF8 MOFs investigated to enhance sensing performance [40]. These incredible properties and performance of MOFs sparked extensive research in the fields of chemical sensors.

To utilize the anticipated properties of CNTs and MOF, Ni-BTC is the isostructural with Zn-BTC and Co-BTC MOFs reported by Yaghi et al. [41]. CNTs have walls of graphene sheets which lead $\pi-\pi$ electron configuration to interact functional group with MOF [42]. In the present investigation, CNT/MOF composite was synthesized and utilized as a chemical gas sensor. SWNTs and MWNTs were functionalized with nitric acid for activation toward sensitivity and used as a backbone for a synthesized framework. The functionalized SWNTs and MWNTs incorporated into Ni-MOF using a solvothermal method, respectively. The new

composite materials Ni-MOF/−OH-SWNTs and Ni-MOF/−OH-MWNTs were employed for chemiresistive detections of SO_2, NO_2, NH_3 and CO analytes at room temperature.

1.1 Experimental details

1.1.1 Functionalization of SWNTs and MWNTs

The functionalization of SWNTs and MWNTs with hydroxyl (−OH) groups was done by adapting chemical methodology [43]. SWNTs (diameter: 1–6 nm, length: 0.5–3 μm) and MWNTs (diameter: 7–16 nm, length: 12–15 μm) were purchased from Sigma-Aldrich. To produce −OH-SWNTs, 1.5 mg SWNTs mixed with 10 ml of concentrated nitric acid and further ultra-sonicated for 60 min with low power at room temperature. After ultrasonication, 100 ml of deionized (DI) water was added into the above mixture. The final solution was dried in an oven at 80 °C for 24 h to evaporate remained water molecules in the precipitate. The same steps were repeated for the preparation of −OH-MWNTs.

1.1.2 Synthesis of pristine Ni-MOF, Ni-MOF/−OH-SWNTs and Ni-MOF/−OH-MWNTs

The pristine Ni-MOF was synthesized using a solvothermal method [44]. Nickel(II) acetate tetrahydrate (0.7 g of 1.41 mol) and 1,3,5 benzenetricarboxylic (0.2 g) mixed with 20 ml of DI and continuously stirred for 30 min at room temperature. Further, the above mixture was transferred in Teflon-coated autoclave and heated up to 170 °C for 12 h. in oven. The resulting green precipitate was cooled at room temp.

For the synthesis of Ni-MOF/−OH-SWNTs and Ni-MOF/−OH-MWNTs, above experiment was followed by the addition of 10 ml −OH-SWNTs and −OH-MWNTs, respectively, into the mixture nickel (II) acetate tetrahydrate and 1,3,5 benzenetricarboxylic. Synthesized materials could be differentiated by their color appearance as shown in Fig. 1. Pristine Ni-MOF resembles a light green color (Fig. 1 (a), Ni-MOF/−OH-SWNTs and Ni-MOF/−OH-MWNTs reflected light and dark gray color, respectively, as shown in optical images Fig. 1 (b) and (c). The synthesized materials were dropped cast on silver electrode-coated flexible polyvinyl chloride sheets having a submicron gap between two electrodes shown in Fig. SI 1.

Fig. 1

Optical image a pristine Ni-MOF, b Ni-MOF/−OH-SWNTs and c Ni-MOF/−OH-MWNTs composite

1.1.3 Instrument details

The XRD patterns were recorded within the range of 5−50° with the help of BRUKER D8 ADVANCE diffractometer using source Cu kα (λ = 1.5406 A°), where voltage and current were held at 40 kV and 40 mA, respectively. The FTIR spectroscopy was done by Alpha ATR, Bruker with ZnSe window having range 4000−500 cm^{-1}. The electrical (I/V) characterization was carried out using a Keithley 4200A semiconductor parameter analyzer (SPA) with a range between -1 and 1 V, whereas surface morphology and roughness were done by FESEM and AFM using Hitachi High-Tech, S-4800 with an operating voltage 15 kV and Park XE-7 system, respectively.

The gas sensing study was carried out using an indigenously developed dynamic gas sensing system (Fig. 2) as reported earlier [42]. For data collection purposes, the gas sensing device was connected to the source meter semiconductor parameter analyzer (Keithley SPA-4200A). Dry air and targeted gas flow were controlled by (Mass Flow Controller (Alicat)) MFC-Non-corrosive and MFC-corrosive, respectively, with a flow rate of 200 SCCM. For desired gas concentrations and storage, Tedlar bag was used. The sensing devices were tested using a ~ 8 cm^2 airtight chamber.

Fig. 2

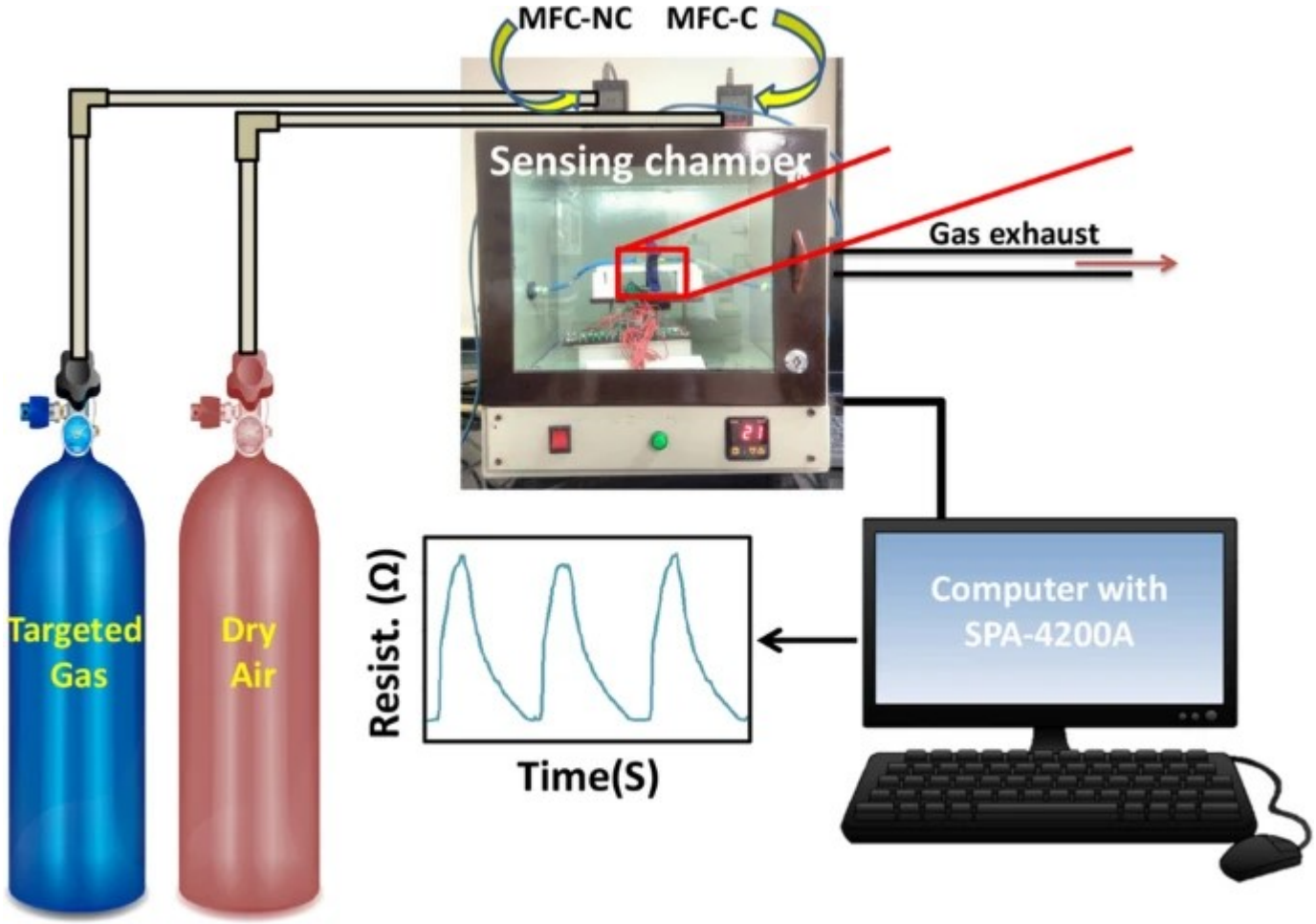

Indigenously developed a dynamic gas sensing system

2 Results and discussions

2.1 Structural, spectroscopic and electrical characterizations

2.1.1 X-ray diffraction (XRD)

Figure 3 (a) and (b) shows the XRD patterns for pristine Ni-MOF and its composite with −OH-SWNTs and −OH-MWNTs named as Ni-MOF/−OH-SWNTs and Ni-MOF/−OH-MWNTs, respectively. All the diffraction patterns of pristine Ni-MOF (Fig. 3 (a)) were confirmed by the reported pattern [45]. DIFFRACTION.EVA software was used for crystallinity calculation. In pristine material, the crystallinity was observed about 40%, whereas 38% and 39%

crystallinity was observed in composite Ni-MOF/−OH-SWNTs and Ni-MOF/−OH-MWNTs, respectively. The intensity of composite materials decreased as compared to pristine material Ni-MOF. It indicates that there are minute changes in the crystal structure of MOF after incorporation of −OH-SWNTs and −OH-MWNTs into Ni-MOF. In full-range XRD patterns peaks look like the same, however, in short-range (Fig. 3 (b)) XRD patterns distinguish the presence of extra graphitic peaks in composite Ni-MOF/−OH-SWNTs (26.189° and 44.759°) and Ni-MOF/−OH-MWNTs (26.251° and 44.814°) compared to pristine Ni-MOF [46]. These eminent peaks confirm the successful incorporation of −OH-SWNTs and −OH-MWNTs in Ni-MOF MOF.

Fig. 3

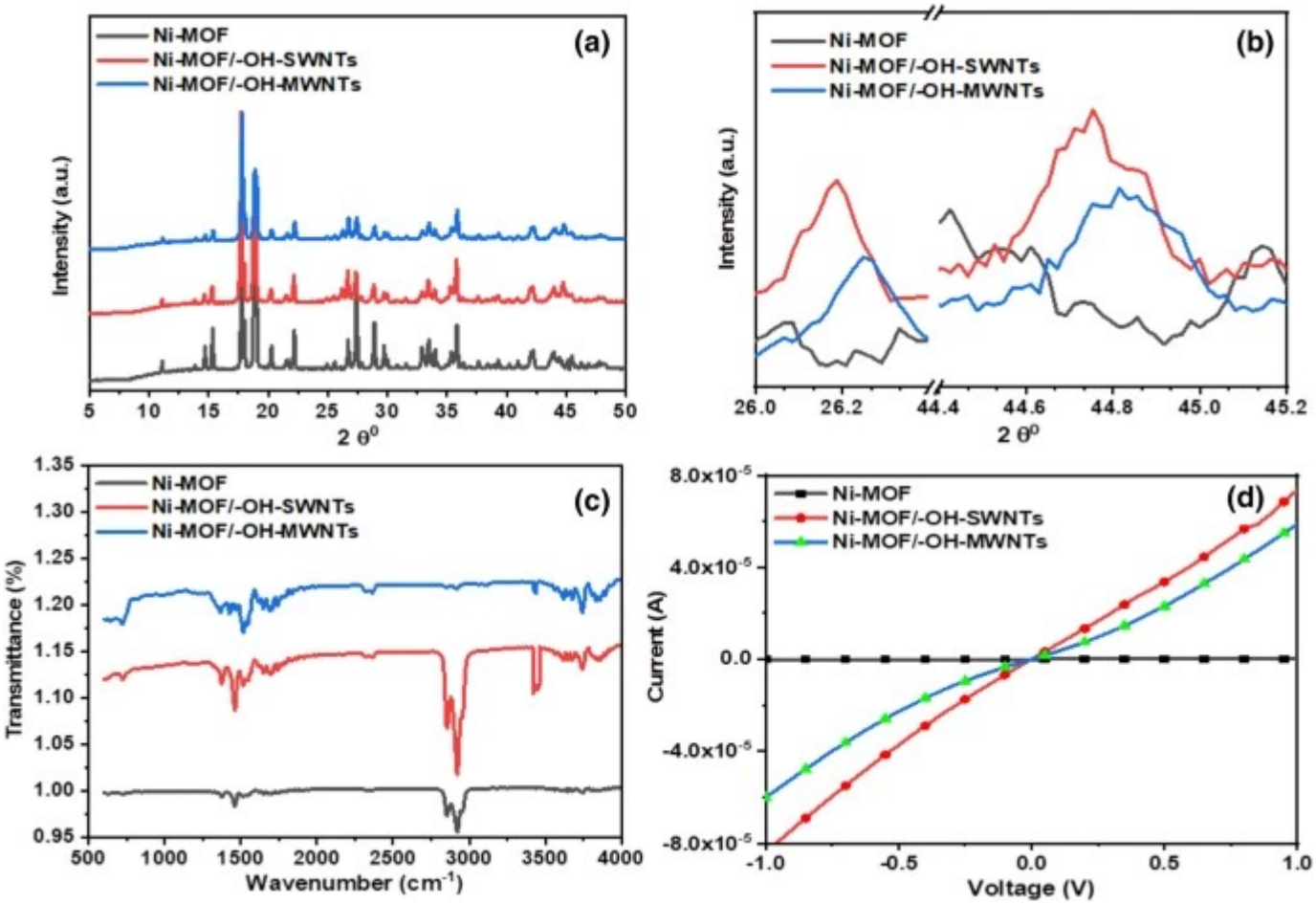

a Full and b short-range XRD pattern recorded for Ni-MOF, Ni-MOF/−OH-SWNTs and Ni-MOF/−OH-MWNTs c FTIR spectra and d I/V measurement of pristine Ni-MOF, Ni-MOF/−OH-SWNTs and Ni-MOF/−OH-MWNTs

The Debye–Scherrer's formula (Eq. 1) was used for calculating crystallite size (D) of pristine Ni-MOF and composite Ni-MOF/−OH-MWNTs and Ni-MOF/−OH-SWNTs materials.

$$D = \frac{0.9\lambda }{{\left({\beta {\text{ cos}}\theta } \right)}},$$

(1)

whereas λ (1.5406 Å) is the wavelength of x-ray source radiation. By using Gauss fitting, full width at half maxima (FWHM) (β) is calculated, pristine Ni-MOF was 0.125 and composite Ni-MOF/−OH-SWNTs and Ni-MOF/−OH-MWNTs were 0.127 and 0.129, respectively. The θ° (12.44°) is the Braggs angle of diffraction. The Ni-MOF exhibits monoclinic crystal system [41]. The calculated crystallite size for pristine Ni-MOF was 66.22 nm and for composite Ni-MOF/−OH-SWNTs and Ni-MOF/−OH-MWNTs were 65.69 nm and 64.68 nm, respectively.

2.1.2 Fourier-transform infrared spectroscopy (FTIR)

Figure 3 (c) shows the resultant peaks of FTIR data for pristine Ni-MOF and composites Ni-MOF/−OH-SWNTs, Ni-MOF/−OH-MWNTs, respectively. The presence of absorption bands at 1350–1650 cm^{-1} reflects the Ni ion coordinated COO moiety [45]. In composite Ni-MOF/−OH-SWNTs and Ni-MOF/−OH-MWNTs peaks reflected at 3432 cm^{-1} attributed stretching vibration of hydroxyl groups (−OH) [47]. The broad and sharp stretching peak was observed at 3033–2800 cm^{-1} for N–H (amine salt) group in pristine Ni-MOF. The intensity of N–H group was gradually decreased with the successive addition of −OH-SWNTs and −OH-MWNTs in Ni-MOF. This evidence confirms the successful formation of Ni-MOF/−OH-SWNTs and Ni-MOF/−OH-MWNTs composites.

2.1.3 Electrical (I/V) characterization

The pristine Ni-MOF resembled $R = \sim 26M\Omega$ (Fig. 3 (d)); however, moderate enhancement has been observed in composite Ni-MOF/−OH-SWNTs ($R = \sim 16K\ \Omega$) and Ni-MOF/−OH-MWNTs ($R = \sim 78\ K\Omega$). From these observations, it can be concluded that bridging network of −OH-SWNTs and −OH-MWNTs helpful to enhance electron transfer in agglomerated microstructure [48]. All measured curves are ohmic in nature with almost symmetric behavior for both composite materials in the negative and positive regions of an applied voltage. This confirms proper connection established between silver electrodes and composite

materials. The formation of −OH-SWNTs and −OH-MWNTs network in Ni-MOF was encouraged to enhance charge transfer in composite materials. The agglomerated micro-network of −OH group-activated SWNTs and MWNTs into Ni-MOF has created free-electron charges. This new network in composite Ni-MOF/−OH-SWNTs and Ni-MOF/−OH-MWNTs materials offered a conductive pathway responsible for charge transport through the micro-network [49, 50].

2.2 Morphological characterizations

2.2.1 Field emission scanning electron microscope (FESEM)

The surface morphology for synthesized materials was characterized using FESEM as shown in Fig. 4 (a), (b) and (c). The pristine Ni-MOF (Fig. 4 (a)) has resulted in an agglomerated microstructure with an average grain size 111 nm. The successfully synthesized composites Ni-MOF/−OH-SWNTs and Ni-MOF/−OH-MWNTs (Fig. 4 (b) and (c), respectively) have resulted in proper formation of networks in microstructure materials. The irregular surface causes more roughness results in a larger contact area with the gaseous analytes. The surface roughness of material is directly proportional to the gas sensitivity [51]. Moreover, here SWNTs and MWNTs created a bridge between agglomerated microstructure and bound them with each other.

Fig. 4

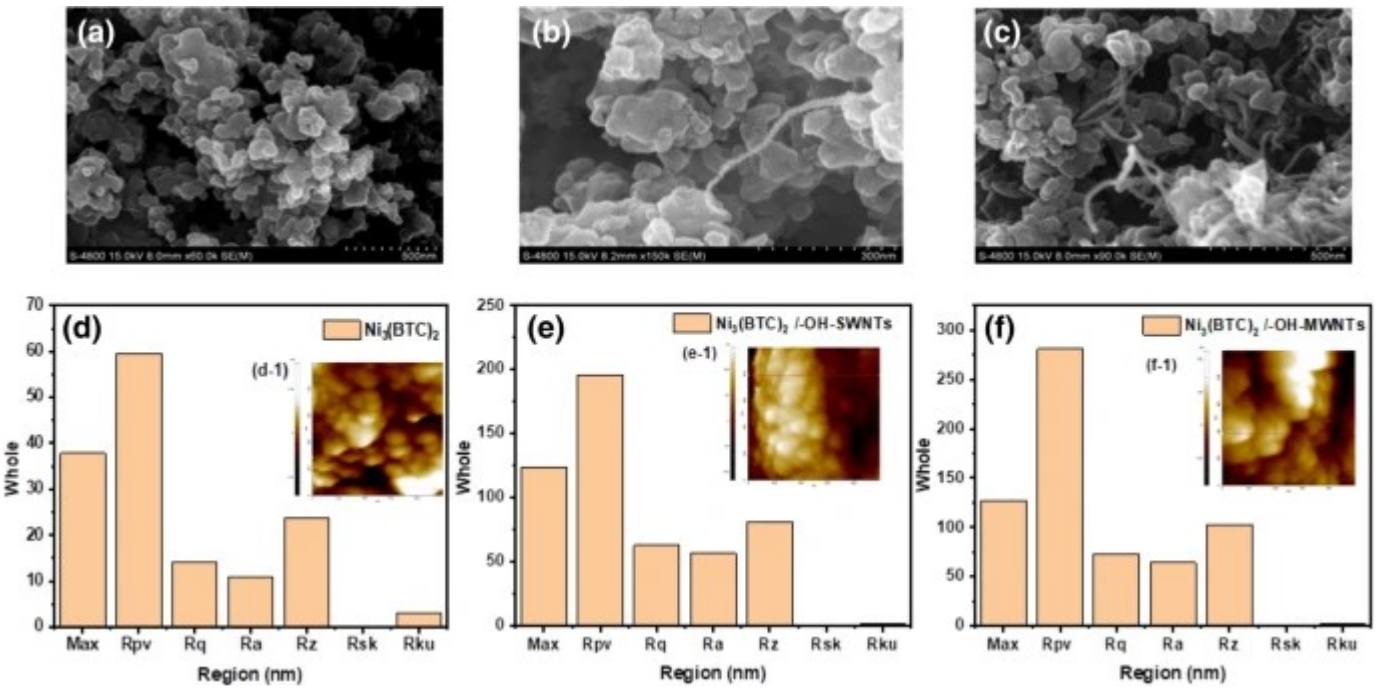

FESEM images (a, b and c) and AFM images (d-1, e-1, and f-1) with surface roughness parameter (d, e and f) for pristine Ni-MOF, Ni-MOF/−OH-SWNTs and Ni-MOF/−OH-MWNTs materials, respectively

2.2.2 Atomic force microscope (AFM)

The AFM characterization was further carried out for the study of materials roughness, the surface area of the prepared materials. Figure 4 (d), (e) and (f) shows the surface roughness parameter of Ni-MOF, composite of Ni-MOF/−OH-SWNTs and Ni-MOF/−OH-MWNTs materials measured from AFM images shown in Fig. 4 (d-1, e-1, f-1), respectively. Composite of Ni-MOF/−OH-SWNTs and Ni-MOF/−OH-MWNTs materials surface exhibited distinct variations in the morphology, compared with pristine Ni-MOF material. Figure 4 (d−f) shows the increment in the surface roughness parameter such as max (maximum roughness), Rpv (peak to valley roughness), Rq (root mean-square roughness), Ra (avrg. roughness), Rz (ten point avrg. roughness), Rsk (skewness) and Rku (avrg. characteristics in height direction).

2.2.3 Gas sensing measurement

The dry air was used to reside initial conditions to achieve baseline, avoid any impact from humidity and balancing targeted gas concentrations. Once the initial condition (baseline) was achieved, targeted gas was exposed to various concentrations. Figure 5 (a) shows dynamic gas sensing of SO_2 gas with various (0.5, 1, 5, 10 and 15 ppm) concentrations for Ni-MOF/−OH-SWNTs and Ni-MOF/−OH-MWNTs sensors. While comparing both composite materials sensing performance, it has been observed that Ni-MOF/−OH-MWNTs took a long time for recovery. Moreover, it was comparably less sensitive than that Ni-MOF/−OH-SWNTs sensors. The −OH-MWNTs holding multi-walled carbon nanotubes with unique pores of honeycomb structure holding gas analyte for a longer time [52]. Besides, both sensors have shown a stable baseline in the presence of dry air. The linear regression (Fig. 5 (b)) equations were $y = 3624.1x + 11{,}007$ ($R^2 = 0.9784$) and $y = 730.86x + 14{,}063$ ($R^2 = 0.9591$), indicating sensing controlled for both Ni-MOF/−OH-SWNTs and Ni-MOF/−OH-MWNTs, respectively.

Fig. 5

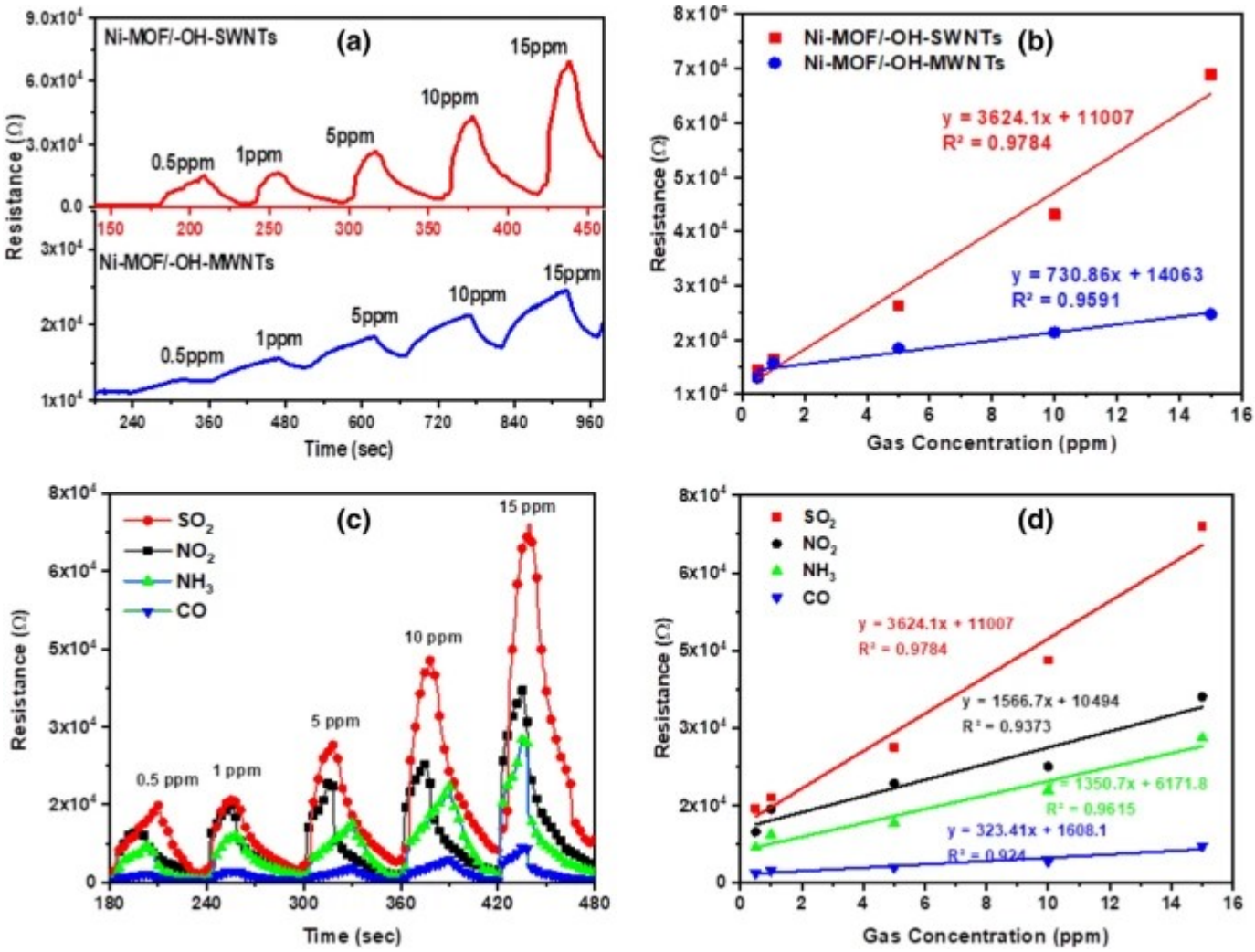

a Dynamic SO_2 sensing for Ni-MOF/−OH-MWNTs and Ni-MOF/−OH-SWNTs sensors, b plot of concentration versus resistance with *R*-squared value, c chemiresistive gas sensing performance and d plot of concentration versus resistance with *R*-squared value for Ni-MOF/−OH-SWNTs toward SO_2, NO_2, NH_3, CO analytes

Figure 5 (c) represents the dynamic gas sensing performance for SO_2, NO_2, NH_3 and CO gases at 0.5–15 ppm concentrations by changing the ohmic resistance of prepared microdevices. Figure 5 (d) shows a noticeable change in *R* squared value based on linear regression equations for SO_2, NO_2, NH_3 and CO gases. It was observed that the prepared Ni-MOF/−OH-SWNTs microdevices showed better sensitivity toward SO_2 analytes compared to other analytes. Figure 6 shows the corresponding results of the sensing measurements. The reproducibility of a sensor plays a crucial role in the gas sensor technology as most important parameters, in the present study Ni-MOF/−OH-SWNTs sensor has shown remarkable reproducibility (Fig. 6 (a))

toward SO_2 analyte at 1 ppm. Response time (10 s) and recovery time (30 s) are one of the key parameters measured for SO_2 analytes at 1 ppm using Ni-MOF/−OH-SWNTs sensor shown in Fig. 6 (b). Ni-MOF/−OH-SWNTs sensor was repeated six times to calculate standard error bar for various gases shown in Fig. 6 (c). It was observed that at lower gas concentrations more deviation compared with higher concentrations. The selectivity performance for Ni-MOF/−OH-SWNTs and Ni-MOF/−OH-MWNTs was investigated and shown in Fig. 6 (d). It was observed that SO_2 is highly selective to Ni-MOF/−OH-SWNTs sensor than other exposed analytes and composite material. The blank −OH-SWNTs and −OH-MWNTs sensing performance is showed in Fig. SI 2 (a) and (b), respectively (supporting information). Moreover, magnified various gases sensing at 0.5 ppm concentrations is shown in Fig. SI 2 (c).

Fig. 6

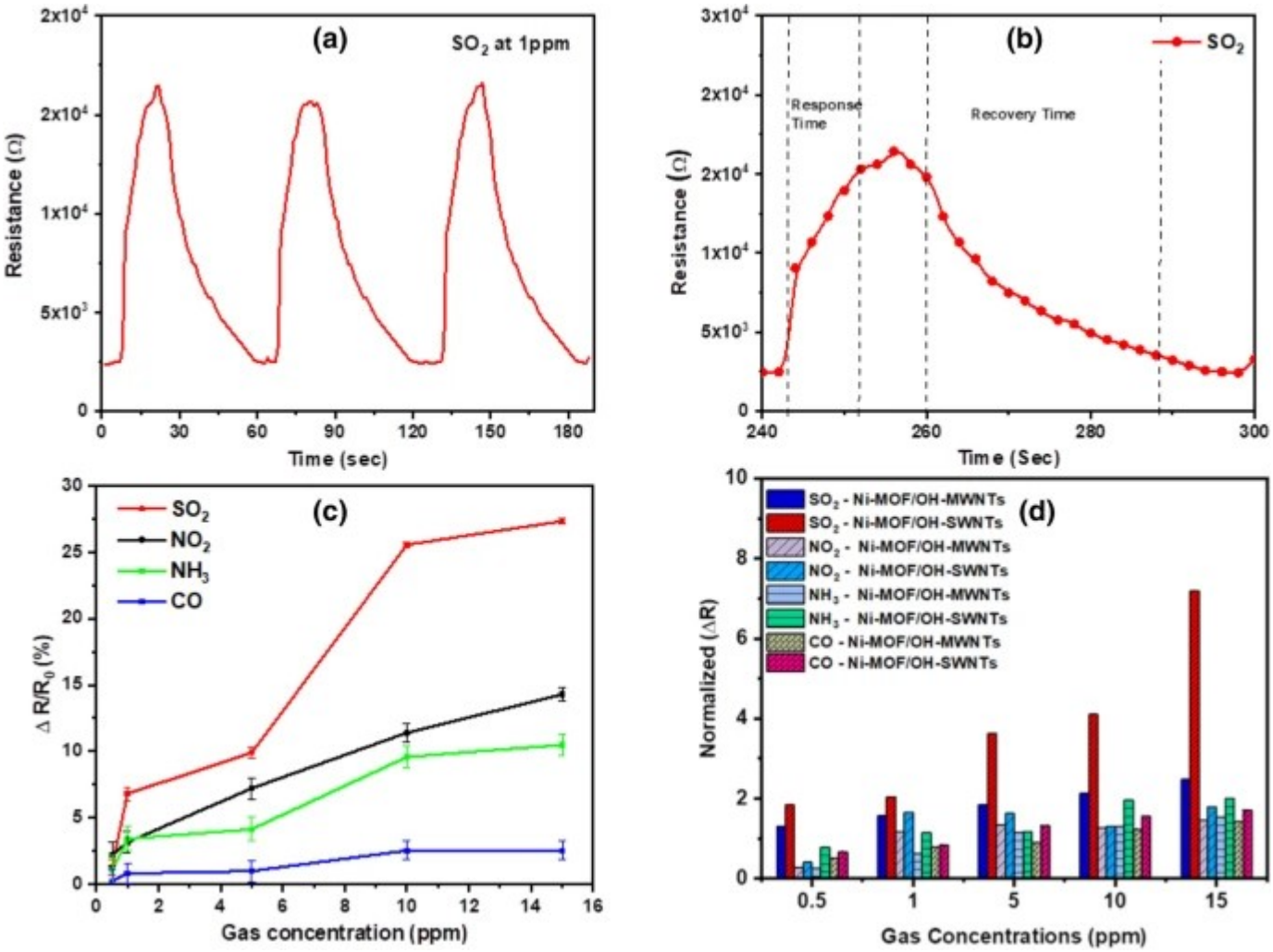

Reproducibility performance of Ni-MOF/−OH-SWNTs sensor toward SO_2 gas at 1 ppm concentration, b response and recovery time for SO_2 analytes using Ni-MOF/−OH-SWNTs composite, c standard

error bar for Ni-MOF/−OH-SWNTs using various gases. d Selectivity performance of Ni-MOF/−OH-MWNTs and Ni-MOF/−OH-SWNTs sensor toward various gas analytes

Table 1 shows the corresponding results of the sensing measurements based on the previously reported literature, and it was observed that Ni-MOF/−OH-SWNTs sensor has shown significant improvements in lower detections and operating conditions toward SO_2 analytes.

Table 1 Reported literature sensing parameters for SO_2 sensor

The sensing mechanism of the reported sensor widely dependent upon zigzag networking in the agglomerated microstructure. The −OH activated SWNTs and MWNTs created a highly sensitive surface network adopting favorable conditions for the transformation of electrons from composite material. In an earlier report [42], Ni-MOF/−OH-SWNTs material represented holes as a majority carrier. When electron donor gas analytes interact with respective material, it will create recombination with each other. Due to this fact, holes get decreased in material, accountable for increment in resistance of the material.

3 Conclusions

The Ni-MOF/−OH-SWNTs and Ni-MOF/−OH-MWNTs composites were successfully synthesized by the solvothermal method. The structural, spectroscopic, morphological characterizations confirmed the successful incorporation of −OH activated SWNTs and MWNTs in Ni-MOF MOF. The I/V characteristic shown a drastic change in the electronic properties of pristine Ni-MOF compared to composite Ni-MOF/−OH-SWNTs and Ni-MOF/−OH-MWNTs materials. −OH-SWNTs and −OH-MWNTs created agglomerated microstructured networks owing to favorable changes in the electrical properties of composite materials. Apart from the characterizations, synthesized materials were tested for various gas analytes such as SO_2, NO_2, NH_3 and CO gases at 0.5−15 ppm concentrations. The response of

the synthesized sensor toward analytes was monitored by observing changes in ohmic resistance of prepared microdevices. A Ni-MOF/−OH-SWNTs sensor has shown remarkable sensor properties in terms of less response time, quick recovery time, good sensitivity, selectivity and better reproducibility. The detection level observed for Ni-MOF/−OH-SWNTs gas sensor toward SO_2 was 0.5 ppm. The reported sensor has undergone ideal properties of the sensor with cost-effectiveness and room temperature operation with ease of material preparation.

References

1. S. Kulkarni, Y. Navale, S. Navale, F. Stadler, N. Ramgir, V. Patil, Hybrid polyaniline-WO3 flexible sensor: a room temperature competence towards NH3 gas. Sensors Actuators B Chem. 288, 279–288 (2019)

Article Google Scholar

2. P.-G. Su, Z.-H. Liao, Fabrication of a flexible single-yarn NH3 gas sensor by layer-by-layer self-assembly of graphene oxide. Mater. Chem. Phys. 224, 349–356 (2019)

Article Google Scholar

3. Y. Fu, J. Li, H. Xu, SnO2 recycled from tin slime for enhanced SO2 sensing properties by NiO surface decoration. Mater. Sci. Semicond. Process. 114, 105073 (2020)

Article Google Scholar

4. P.W. Sayyad, S.S. Khan, N.N. Ingle, G.A. Bodkhe, T. Al-Gahouari, M.M. Mahadik, S.M. Shirsat, M.D. Shirsat, Chemiresistive SO 2 sensor: graphene oxide (GO) anchored poly (3, 4-ethylenedioxythiophene): poly (4styrenesulfonate)(PEDOT: PSS). Appl. Phys. A 126, 1–8 (2020)

Article Google Scholar

5. T. Al-Gahouari, G. Bodkhe, P. Sayyad, N. Ingle, M. Mahadik, S.M. Shirsat, M. Deshmukh, N. Musahwar, M. Shirsat, Electrochemical sensor: L-cysteine induced selectivity enhancement of electrochemically reduced graphene oxide-multiwalled carbon nanotubes hybrid for detection of lead (Pb2+) ions. Front. Mater. 7, 68 (2020)

Article ADS Google Scholar

6. I. Obot, I.B. Onyeachu, S.A. Umoren, M.A. Quraishi, A.A. Sorour, T. Chen, N. Aljeaban, Q. Wang, High temperature sweet corrosion and inhibition in the oil and gas industry: progress, challenges and future perspectives. J. Petrol. Sci. Eng. 185, 106469 (2020)

Article Google Scholar

7. M. Mahadik, H. Patil, G. Bodkhe, N. Ingle, P. Sayyad, T. Al-Gahaouri, S.M. Shirsat, M. Shirsat, EDTA modified PANI/GO composite based detection of Hg (II) ions. Front. Mater. 7, 81 (2020)

Article ADS Google Scholar

8. K. Park, S. Choi, H.Y. Chae, C.S. Park, S. Lee, Y. Lim, H. Shin, J.J. Kim, An energy-efficient multimode multichannel gas-sensor system with learning-based optimization and self-calibration schemes. IEEE Trans. Industr. Electron. 67, 2402–2410 (2019)

Article Google Scholar

9. Zaza, F.; Pallozzi, V.; Serra, E. Optimization of working conditions for perovskite-based gas sensor devices by multiregression analysis. J. Nanotechnol. 2019.

10. L. Zhu, W. Zeng, Room-temperature gas sensing of ZnO-based gas sensor: a review. Sens. Actuators A 267, 242–261 (2017)

Article Google Scholar

11. K. Eslami Jahromi, Q. Pan, A. Khodabakhsh, C. Sikkens, P. Assman, S.M. Cristescu, P.M. Moselund, M. Janssens, B.E. Verlinden, F.J. Harren, A broadband mid-infrared trace gas sensor using supercontinuum light source: applications for real-time quality control for fruit storage. Sensors 19, 2334 (2019)

Article Google Scholar

12. Vashpanov, Y.; Son, J.-Y.; Heo, G.; Kwack, K.-D. In *Tilte*2020; IOP Publishing.

13. M.D. Shirsat, M.A. Bangar, M.A. Deshusses, N.V. Myung, A. Mulchandani, Polyaniline nanowires-gold nanoparticles hybrid network based chemiresistive hydrogen sulfide sensor. Appl. Phys. Lett. 94, 083502 (2009)

Article ADS Google Scholar

14. Y. Seekaew, A. Wisitsoraat, D. Phokharatkul, C. Wongchoosuk, Room temperature toluene gas sensor based on TiO2 nanoparticles decorated 3D graphene-carbon nanotube nanostructures. Sensors Actuators B Chem. 279, 69–78 (2019)

Article Google Scholar

15. Y. Deng, *Sensing Mechanism and Evaluation Criteria of Semiconducting Metal Oxides Gas Sensors* (Springer, In Semiconducting Metal Oxides for Gas Sensing, 2019), pp. 23–51

Book Google Scholar

16. H. Kharat, K. Kakde, P. Savale, K. Datta, P. Ghosh, M. Shirsat, Synthesis of polypyrrole films for the development of ammonia sensor. Polym. Adv. Technol. 18, 397–402 (2007)

Article Google Scholar

17. F. Loghin, A. Abdellah, A. Falco, M. Becherer, P. Lugli, A. Rivadeneyra, Time stability of carbon nanotube gas sensors. Measurement 136, 323–325 (2019)

Article ADS Google Scholar

18. P.W. Sayyad, N.N. Ingle, T. Al-Gahouari, M.M. Mahadik, G.A. Bodkhe, S.M. Shirsat, M.D. Shirsat, Sensitive and selective detection of Cu2+ and Pb2+ ions using Field Effect Transistor (FET) based on L-Cysteine anchored PEDOT: PSS/rGO composite. Chem. Phys. Lett. 761, 138056 (2020)

Article Google Scholar

19. M. Patil, V. Ganbavle, K. Rajpure, H. Deshmukh, S. Mujawar, Fast response and highly selective nitrogen dioxide gas sensor based on Zinc Stannate thin films. Mater. Sci. Energy Technol. 3, 36–42 (2020)

Google Scholar

20. G. Neri, A. Bonavita, C. Milone, S. Galvagno, Role of the Au oxidation state in the CO sensing mechanism of Au/iron oxide-based gas sensors. Sensors Actuators B Chem. 93, 402–408 (2003)

Article Google Scholar

21. R.K. Jha, V. Singh, J. Sinha, S. Avasthi, N. Bhat, CVD grown cuprous oxide thin film based

high performance chemiresistive ammonia gas sensors. IEEE Sens. J. 19, 11759–11766 (2019)

Article ADS Google Scholar

22. M.A. Deshmukh, H.K. Patil, G.A. Bodkhe, M. Yasuzawa, P. Koinkar, A. Ramanavicius, S. Pandey, M.D. Shirsat, EDA modified PANI/SWNTs nanocomposite for determination of Ni (II) metal ions. Colloids Surf. A 537, 303–309 (2018)

Article Google Scholar

23. M.A. Deshmukh, H.K. Patil, G.A. Bodkhe, M. Yasuzawa, P. Koinkar, A. Ramanaviciene, M.D. Shirsat, A. Ramanavicius, EDTA-modified PANI/SWNTs nanocomposite for differential pulse voltammetry based determination of Cu (II) ions. Sensors Actuators B Chem. 260, 331–338 (2018)

Article Google Scholar

24. W. Zhang, S. Cao, Z. Wu, M. Zhang, Y. Cao, J. Guo, F. Zhong, H. Duan, D. Jia, High-performance gas sensor of Polyaniline/Carbon nanotube composites promoted by interface engineering. Sensors 20, 149 (2020)

Article Google Scholar

25. T. Seesaard, T. Kerdcharoen, C. Wongchoosuk, *Hybrid Materials with Carbon Nanotubes for Gas Sensing* (Elsevier, In Semiconductor Gas Sensors, 2020), pp. 185–222

Google Scholar

26. H.K. Patil, M.A. Deshmukh, G.A. Bodkhe, S.M. Shirsat, K. Asokan, M.D. Shirsat, Reinforcement of polyaniline and poly-(o-toluidine) with SWNTs and tuning of their physicochemical properties by heavy ion beams. Appl. Phys. A 124, 491 (2018)

Article ADS Google Scholar

27. Reed, D.; Xiao, D. J.; Jiang, H. Z.; Chakarawet, K.; Oktawiec, J.; Long, J. R. Biomimetic O2 adsorption in an iron metal–organic framework for air separation. Chem. Sci. 2020.

28. G.A. Bodkhe, M.A. Deshmukh, H.K. Patil, S.M. Shirsat, V. Srihari, K.K. Pandey, G. Panchal, D.M. Phase, A. Mulchandani, M.D. Shirsat, Field effect transistor based on proton conductive metal organic framework (CuBTC). J. Phys. D Appl. Phys. 52, 335105 (2019)

Article Google Scholar

29. D. Li, M. Kassymova, X. Cai, S.-Q. Zang, H.-L. Jiang, Photocatalytic CO2 reduction over metal-organic framework-based materials. Coord. Chem. Rev. 412, 213262 (2020)

Article Google Scholar

30. N. Ingle, P. Sayyad, G. Bodkhe, M. Mahadik, A.-G. Theeazen, S. Shirsat, M.D. Shirsat, ChemFET Sensor: nanorods of nickel-substituted Metal-Organic framework for detection of SO 2. Appl. Phys. A 126, 1–9 (2020)

Article Google Scholar

31. Q. Yang, B. Wang, Y. Chen, Y. Xie, J. Li, An anionic In (III)-based metal-organic framework with Lewis basic sites for the selective adsorption and separation of organic cationic dyes. Chin. Chem. Lett. 30, 234–238 (2019)

Article Google Scholar

32. Souza, B. E.; Donà, L.; Titov, K.; Bruzzese, P.; Zeng, Z.; Zhang, Y.; Babal, A. S.; Möslein, A. F.; Frogley, M. D.; Wolna, M. Elucidating the drug release from metal-organic framework

nanocomposites via in situ synchrotron microspectroscopy and theoretical modelling. ACS Appl. Mater. Interfaces 2020.

33. Connolly, B. M.; Madden, D. G.; Wheatley, A. E.; Fairen-Jimenez, D. Shaping the future of fuel: Monolithic metal-organic frameworks for high-density gas storage. J. Am. Chem. Soci. 2020.

34. S.G. Surya, S. Bhanoth, S.M. Majhi, Y.D. More, V.M. Teja, K.N. Chappanda, A silver nanoparticle-anchored UiO-66 (Zr) metal–organic framework (MOF)-based capacitive H 2 S gas sensor. CrystEngComm 21, 7303–7312 (2019)

Article Google Scholar

35. X. Chen, Y. Lyu, Z. Wang, X. Qiao, B.C. Gates, D. Yang, Tuning Zr12O22 node defects as catalytic sites in the metal-organic framework hcp UiO-66. ACS Catalysis 10, 2906–2914 (2020)

Article Google Scholar

36. Farha, O. K.; Eryazici, I.; Jeong, N. C.; Hauser, B. G.; Wilmer, C. E.; Sarjeant, A. A.; Snurr, R. Q.; Nguyen, S. T.; Yazaydın, A. O. z. r.; Hupp, J. T. Metal–organic framework materials with ultrahigh surface areas: is the sky the limit? *Journal of the American Chemical Society* 2012, *134*, 15016–15021.

37. C.R. Wade, M. Dincă, Investigation of the Synthesis, Activation, and Isosteric Heats of CO_2 Adsorption of the Isostructural Series of Metal-Organic Frameworks M_3 $(BTC)_2$ (M= Cr (Fe, Ni, Cu, Mo, Ru), (2012).

Book Google Scholar

38. Song, Y.; Khudozhitkov, A. E.; Lee, J.; Kang, H.; Kolokolov, D. I.; Stepanov, A. G.; Yoon, M.

Transformation of a proton insulator to a conductor via reversible amorphous to crystalline structure transformation of MOFs. Chem. Commun. 2020.

39. Q.-Q. Huang, Y.-J. Lin, R. Zheng, W.-H. Deng, C. Kashi, P.N. Kumar, G.-E. Wang, G. Xu, Tunable electrical conductivity of a new 3D MOFs: Cu-TATAB. Inorg. Chem. Commun. 105, 119–124 (2019)

Article Google Scholar

40. T.T. Tung, M.T. Tran, J.-F. Feller, M. Castro, T. Van Ngo, K. Hassan, M.J. Nine, D. Losic, Graphene and metal organic frameworks (MOFs) hybridization for tunable chemoresistive sensors for detection of volatile organic compounds (VOCs) biomarkers. Carbon 159, 333–344 (2020)

Article Google Scholar

41. O. Yaghi, H. Li, T. Groy, Construction of porous solids from hydrogen-bonded metal complexes of 1, 3, 5-benzenetricarboxylic acid. J. Am. Chem. Soc. 118, 9096–9101 (1996)

Article Google Scholar

42. N. Ingle, S. Mane, P. Sayyad, G. Bodkhe, T. Al-Gahouari, M. Mahadik, S. Shirsat, M.D. Shirsat, Sulfur dioxide (SO 2) detection using composite of Nickel benzene carboxylic (Ni 3 BTC 2) and OH-functionalized single walled carbon nanotubes (OH-SWNTs). Front. Mater. 7, 93 (2020)

Article ADS Google Scholar

43. H. Hu, B. Zhao, M.E. Itkis, R.C. Haddon, Nitric acid purification of single-walled carbon nanotubes. J. Phys. Chem. B 107, 13838–13842 (2003)

Article Google Scholar

44. L.-N. Jin, Q. Liu, W.-Y. Sun, Room temperature solution-phase synthesis of flower-like nanostructures of [Ni3 (BTC) 2· 12H2O] and their conversion to porous NiO. Chin. Chem. Lett. 24, 663–667 (2013)

Article Google Scholar

45. Lestari, W.; Winarni, I.; Rahmawati, F. In *Tilte*2017; IOP Publishing.

46. L. Xing, F. Du, J.-J. Liang, Y.-S. Chen, Q.-L. Zhou, Preparation of Pt/SWNTs for heterogeneous asymmetric hydrogenation of ethyl pyruvate. J. Mol. Catal. A: Chem. 276, 191–196 (2007)

Article Google Scholar

47. S. Liang, G. Li, R. Tian, Multi-walled carbon nanotubes functionalized with a ultrahigh fraction of carboxyl and hydroxyl groups by ultrasound-assisted oxidation. J. Mater. Sci. 51, 3513–3524 (2016)

Article ADS Google Scholar

48. P.-C. Ma, M.-Y. Liu, H. Zhang, S.-Q. Wang, R. Wang, K. Wang, Y.-K. Wong, B.-Z. Tang, S.-H. Hong, K.-W. Paik, Enhanced electrical conductivity of nanocomposites containing hybrid fillers of carbon nanotubes and carbon black. ACS Appl. Mater. Interfaces. 1, 1090–1096 (2009)

Article Google Scholar

49. H.H. Choi, J. Lee, K.-Y. Dong, B.-K. Ju, W. Lee, Gas sensing performance of composite materials using conducting polymer/single-walled carbon nanotubes. Macromol. Res. 20, 143–146 (2012)

Article Google Scholar

50. Eletskii, A. V.; Knizhnik, A. A.; Potapkin, B. V. e.; Kenny, J. M. Electrical characteristics of carbon nanotube-doped composites. Phys.-Uspekhi 2015, *58*, 209.

51. S. Thirumalairajan, K. Girija, V.R. Mastelaro, N. Ponpandian, Surface morphology-dependent room-temperature LaFeO3 nanostructure thin films as selective NO2 gas sensor prepared by radio frequency magnetron sputtering. ACS Appl. Mater. Interfaces. 6, 13917–13927 (2014)

Article Google Scholar

52. S. Mao, G. Lu, J. Chen, Nanocarbon-based gas sensors: progress and challenges. J. Mater. Chem. A 2, 5573–5579 (2014)

Article Google Scholar

53. Yang, J.; Cheng, F.; Zhu, Z.; Feng, J.; Xue, M.; Meng, Z.; Qiu, L. Enhanced gas sensor based on SiO2@ mesoporous MCM-41 core-shell nanocomposites for SO2 visual detection. Analyst 2020.

54. Y. Liu, X. Xu, Y. Chen, Y. Zhang, X. Gao, P. Xu, X. Li, J. Fang, W. Wen, An integrated micro-chip with Ru/Al2O3/ZnO as sensing material for SO2 detection. Sensors Actuators B: Chem. 262, 26–34 (2018)

Article Google Scholar

55. Q. Zhou, W. Zeng, W. Chen, L. Xu, R. Kumar, A. Umar, High sensitive and low-concentration sulfur dioxide (SO2) gas sensor application of heterostructure NiO-ZnO nanodisks. Sensors Actuators B Chem. 298, 126870 (2019)

Article Google Scholar

56. W. Li, J. Guo, L. Cai, W. Qi, Y. Sun, J.-L. Xu, M. Sun, H. Zhu, L. Xiang, D. Xie, UV light irradiation enhanced gas sensor selectivity of NO2 and SO2 using rGO functionalized with hollow SnO2 nanofibers.Sensors Actuators B Chem. 290, 443–452 (2019)

Article Google Scholar

57. Su, H. C.; Tran, T.-T.; Bosze, W.; Myung, N. V. Chemiresistive sensor arrays for detection of air pollutants based on carbon nanotubes functionalized with porphyrin and phthalocyanine derivatives. Sensors Actuators Reports 2020, 100011.

58. U. Chaitra, A.M. Ali, A.E. Viegas, D. Kekuda, K.M. Rao, Growth and characterization of undoped and aluminium doped zinc oxide thin films for SO2 gas sensing below threshold value limit. Appl. Surf. Sci. 496, 143724 (2019)

Article Google Scholar

59. G. Jung, Y. Jeong, Y. Hong, M. Wu, S. Hong, W. Shin, J. Park, D. Jang, J.-H. Lee, SO2 gas sensing characteristics of FET-and resistor-type gas sensors having WO3 as sensing material. Solid-State Electronics 165, 107747 (2020)

Article ADS Google Scholar

60. M. Drobek, J.-H. Kim, M. Bechelany, C. Vallicari, A. Julbe, S.S. Kim, MOF-based membrane encapsulated ZnO nanowires for enhanced gas sensor selectivity. ACS Appl. Mater. Interfaces. 8, 8323–8328 (2016)

Article Google Scholar

61. W. Zhou, Y.-P. Wu, J. Zhao, W.-W. Dong, X.-Q. Qiao, D.-F. Hou, X. Bu, D.-S. Li, Efficient gas-sensing for formaldehyde with 3D hierarchical Co3O4 derived from Co5-based MOF microcrystals. Inorg. Chem. 56, 14111–14117 (2017)

Article Google Scholar

Acknowledgements

The authors are thankful to the Inter University Accelerator Center (IUAC), New Delhi, for providing financial and material science beamline with FESEM facilities through IUAC-UGC project having UFR-62320 & UFR-62321. Also thankful to DST-SERB (sanction no. EEQ/2017/000645), UGC-DAE CSR (RRCAT) Indore (Project No. CSR-IC-BL66/CSR-183/2016-17/847), UGC-SAP programme (F.530/16/DRS-1/2016 (SAP-II), dt. 16-04-2016), DST-FIST (Project No. No. SR/FST/PSI-210/2016(C) dtd. 16/12/2016), Rashtria Uchachatar Shiksha Abhiyan (RUSA), Government of Maharashtra for providing characterization facilities. Also thankful to Dr. Saif A. Khan, IUAC, New Delhi.

Author information

Authors and Affiliations

RUSA Centre for Advanced Sensor Technology, Department of Physics, Dr. Babasaheb Ambedkar, Marathwada University, Aurangabad, Maharashtra, India, 431004
Nikesh Ingle, Pasha Sayyad, Megha Deshmukh, Gajanan Bodkhe, Manasi Mahadik, Theeazen Al-Gahouari & Mahendra D. Shirsat

Department of Electronics & Telecommunication Engineering, Jawaharlal Nehru Engineering College, Aurangabad, Maharashtra, India, 431001
Sumedh Shirsat

Corresponding author

Correspondence to Mahendra D. Shirsat.

Additional information

Publisher's Note

Supplementary Information

Below is the link to the electronic supplementary material.

Supplementary file1 (DOCX 225 kb)

Rights and permissions

About this article

Cite this article

Ingle, N., Sayyad, P., Deshmukh, M. *et al.* A chemiresistive gas sensor for sensitive detection of SO_2 employing Ni-MOF modified –OH-SWNTs and –OH-MWNTs. *Appl. Phys. A* 127, 157 (2021). https://doi.org/10.1007/s00339-021-04288-0

Received	Accepted	Published
19 November 2020	06 January 2021	02 February 2021

DOI
https://doi.org/10.1007/s00339-021-04288-0

Share this article

Anyone you share the following link with will be able to read this content:

Get shareable link

Keywords

Metal–organic frameworks (MOFs) Carbon nanotubes (CNTs)

Chemiresistive sensor Sulfur dioxide (SO_2) Sensitivity and selectivity